

Sequential binding-unbinding based specific interactions highlight exchange dynamics and size distribution of condensates*

Bhanjan Debnath and Parag Katira[†]

Department of Mechanical Engineering, San Diego State University, CA, 92182, USA

Understanding the mechanisms of formation of organelles and biomolecular condensates via liquid-liquid phase separation is a topic of great interest. It is reasonable to assume that the formation of protein-specific condensates inside a crowded, multicomponent cellular environment requires specific protein-protein interactions with lifetimes longer than non-specific protein-protein interactions. These longer-lived, specific interactions can arise through complex protein binding and unbinding pathways. In this work, we investigate single-step and sequential multi-step mechanisms for protein binding-unbinding interactions and model the lifetimes of such interactions in a heuristic manner. We show that while similar average interaction lifetimes can be achieved when binding-unbinding follows a single-step or a sequential multi-step process, the two processes result in two distinct lifetime distributions: exponential and truncated power-law, respectively. We then combine this model with Brownian dynamics simulations to elucidate the impact of these distinct lifetime distributions on condensate dynamics. Our model qualitatively captures important features of condensates, such as their fluidic nature, aging in protein interactions and its impact on the exchange dynamics, and the size distribution of condensates. In a nutshell, our model unravels how specificity in protein binding-unbinding interaction pathways, resulting in unique interaction lifetime distributions, is a key factor shaping the physical properties of biomolecular condensates.

Introduction—Liquid-liquid phase separation, formation of organelles and biomolecular condensates have been observed in numerous biological processes inside cells [1–3]. Such membraneless compartments, for example, P-granules and stress granules exhibit droplet-shaped liquid-like features [4, 5]. The most common features include internal rearrangement, material exchange between the condensates and the surrounding, coarsening leading to varying condensate size distributions, dissolution, etc. [6–12]. These features are essential for crucial biological functions, such as signaling and maintaining a biochemical environment within organelles by sequestering unwanted molecules. But, not all condensates need to remain in a liquid-like state. It has been observed that there is a transition from the liquid to the gel-like state as the condensate ages or matures through solvent expulsion [13–16]. These transitions are linked to cataract, pathological aggregation, and neurodegenerative diseases such as amyotrophic lateral sclerosis and Parkinson’s disease [5, 17–19]. The increasing number of biological processes in which biomolecular condensates have been discovered, coupled with limited success in explaining their presence or impact during these processes, fuels the significant intrigue and interest in biomolecular condensates [2, 3].

A body of work has attempted to explain the mechanisms underlying key features of biomolecular condensate. It is well explored how strong and weak interactions among proteins containing intrinsically disordered regions (IDRs) are responsible for condensate formation [20–23]. A few studies have explored the role of strong interactions between relatively rigid structure protein regions and their role in condensate formation and dynam-

ics [23]. Several factors influence the binding affinity and specificity in biomolecular interactions resulting in phase separation, including electrostatic and other long-range interactions, multivalency, weak bond formation (for example, hydrogen bond), conformational selections, and solvent-solute interactions [15, 23]. Although there is progress in current understanding, the factors influencing the fluidic nature of condensates, exchange dynamics, aging, and size distributions remain to be fully elucidated. One plausible factor commonly contributing to these features can be ‘the lifetime of protein interactions’ within a condensate, which, although seemingly intuitive, is less questioned and can play a crucial role in regulating the dynamics.

We define the lifetime of interactions as the duration for which any two protein molecules remain to be continuously adhered to each other when they interact. If these durations are extremely long, this may indicate that the condensates behave as solids, whereas very short-lived interactions may not allow the formation of stable condensates. It is apparent that protein binding sites, binding strengths, thermal fluctuations, and the strengths of external forces (if present) impact these durations. However, the following key questions remain: 1) how the mechanisms of binding and unbinding between interacting proteins give rise to distinct interaction lifetimes, and 2) how the distributions of these interaction lifetimes affect the dynamics of condensate formation while maintaining the specificity between the interacting proteins.

Over the decades, various mechanisms for binding and unbinding interactions between proteins and between proteins and surfaces have been proposed [24–27]. Binding-unbinding has generally been considered as a first-order reversible reaction pathway, leading to exponential lifetime distributions in the equilibrium limit. In the case of a small number of protein molecules interact-

* Supplementary information (SI) available

[†] Corresponding author: bdebnath@sdsu.edu; pkatira@sdsu.edu

ing with a surface having a large number of binding sites, the binding-unbinding events can be approximated as a Poisson process. However, the former may not be true if binding-unbinding does not follow a single-step pathway [28–32]. In such cases, it has been reported earlier that the lifetime distributions are non-exponential. In the context of condensate formation, the dynamics of binding and unbinding can be of significant relevance, as it can drive the specificity in protein interactions [33], thus contributing to the formation of protein-specific condensates. Here, we aim to highlight whether specific binding-unbinding interactions can also influence the features of these condensates.

In recent years, the sticker-spacer class of models has been used to predict features of condensates [21, 22, 34, 35]. Although this model effectively captures phase separation, the question of binding-unbinding pathways remains open. A recent study uses this model to explain the exchange dynamics between the dense and dilute phases [36]. However, it is not clear whether the same model can predict different size distributions, particularly exponential and power-law as observed in experiments, in different protein-specific systems [7, 8]. The exchange events would be reduced when condensates exhibit gel-like features. The coexistence of liquid and gel-like states as condensates mature has been shown using the sticker-spacer model [37] and molecular dynamics (MD) simulations [38]; but, the liquid-like features and the exchange dynamics are not captured in the early stage of phase separation.

We hypothesize that a trade-off between high specificity in protein interactions, resulting in longer interaction lifetimes and a gel-like state, with the fluidic nature of condensates in the early stage of phase separation, relies on unique interaction mechanisms beyond single-step binding-unbinding processes or even multi-step interactions that lead to non-exponentially distributed interaction lifetimes. In this present work, we focus on modeling selective interactions between proteins that can lead to distinct interaction lifetime signatures. We show the emergence of two distinct lifetime distributions from single-step and multi-step binding-unbinding interactions, providing physical insights into interactions with high specificity. Building on the former, we use a minimal hybrid framework that integrates these interaction lifetimes with Brownian dynamics to simulate the motion of protein molecules and condensates. Our model captures key features of condensates and demonstrates how specific binding-unbinding interaction pathways influence condensate behavior, highlighting the link between the specificity in protein interaction pathways and condensate dynamics.

Model— Except for long-range and electrostatic attractions, the high specificity in protein-protein interactions can arise because of their backbone shape and ‘extensive and modular side-chain hydrogen-bond networks’ [33, 39]. In interactions, these networks become gradually accessible for binding and unbinding through conforma-

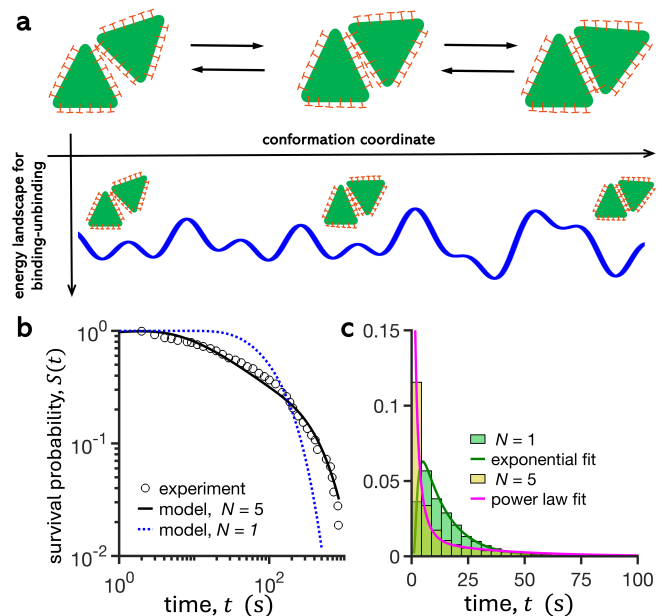


FIG. 1. (a) Schematic of sequential binding-unbinding mechanism. Binding and unbinding through conformational changes occur in a sequential manner on the conformation coordinate. (b) Comparison of model predictions with experiments of Armstrong *et al.* [31]. Survival probability $S(t)$ with time t for multi-step and single-step binding-unbinding mechanisms. For the same mean lifetime $\tau_m = 130$ s, the best fits are $\tilde{C} = 0.03$ and $\tilde{C} = 0.0038$ for the total number of probable conformational changes $N = 5$ and $N = 1$, respectively, where $\tilde{C} = C/\alpha$ and α represents one square unit of conformational changes per second. (c) The lifetime distributions (PDF = $-dS/dt$) for $N = 5$ and $N = 1$; the choices of \tilde{C} are such that the mean lifetime of both distributions is the same. In (c), for a chosen mean lifetime $\tau_m = 15$ s, $\tilde{C} = 0.3$ and $\tilde{C} = 0.034$ for $N = 5$ and $N = 1$, respectively.

tional changes [40, 41]. These selective interactions are often coined as ‘interaction specificity’, especially when the protein molecules are in a heterogeneous and multicomponent chemical environment [23]. Modeling such intricate interactions when two protein molecules are in close proximity is challenging, prompting us to adopt a heuristic approach. We assume that binding and unbinding through conformational changes occur in a sequential manner (see Fig. 1a). For simplicity, we further assume that the probability in a future conformational bound state $n_{(t+\Delta t)}$ depends on the current bound state n_t , i.e., $\mathcal{P}(n_{(t+\Delta t)}|n_t, n_{(t-\Delta t)}, n_{(t-2\Delta t)}, \dots, n_{t=0}) = \mathcal{P}(n_{(t+\Delta t)}|n_t)$. If there is a bias that favors certain bound states, then the system evolves according to the equation:

$$\begin{aligned} \frac{\partial \mathcal{P}(n, t)}{\partial t} + \frac{\partial}{\partial n} [\mathcal{U}(n, t) \mathcal{P}(n, t)] \\ = \frac{\partial}{\partial n} \left[\mathcal{C}(n, t) \frac{\partial \mathcal{P}(n, t)}{\partial n} \right], \end{aligned} \quad (1)$$

where $\mathcal{U}(n, t)$ is the drift and $\mathcal{C}(n, t)$ is the diffusivity associated with conformational fluctuations. Both can be re-

lated to the energy barrier for transitioning between different conformational bound states and the depth of the energy well at each conformational state. More work is required to generate the exact energy landscapes for these specific interactions [42–44], and develop relations for $\mathcal{U}(n, t)$ and $\mathcal{C}(n, t)$ in connection with these energy landscapes, which is beyond the scope of the present work. The survival probability, $S(t) = \int \mathcal{P}(n, t) dn$, represents the likelihood that the bound protein molecules remain attached after a period of time. Therefore, $(-dS/dt)$ directly corresponds to a distribution of lifetimes of such specific interactions. We note in passing that we prefer to decouple the effects of other long-range and electrostatic interactions, and therefore, exclude them from the present model.

As Eq. 1 resembles the standard advection-diffusion equation, an exact solution of Eq. 1 can be obtained for a special case without drift and no variation of \mathcal{C} with n and t . This corresponds to a uniform energy landscape, which may not always be true. However, for simplicity, we adopt this case to test the potential and predictability of the model. For this special case and a total number of probable conformational changes N , $S(t)$ is obtained as (see the supplementary information (SI) section SI1)

$$S(t) = \frac{4}{\pi} \sum_{\ell=1}^{\infty} \left\{ \frac{1}{(2\ell-1)} \sin \left[\frac{(2\ell-1)\pi}{2N} \right] \times \exp \left[-\mathcal{C} \left(\frac{(2\ell-1)\pi}{2N} \right)^2 t \right] \right\}. \quad (2)$$

This model captures the truncated power-law trend observed in experiments reasonably well when the binding-unbinding is considered as a multi-step mechanism ($N > 1$), shown in Fig. 1b. The experimental data in this case represent the interaction of proteins (fibrinogen) with a surface (glass) [31]. However, when the binding-unbinding is considered as a single-step mechanism ($N = 1$), the model instead predicts an exponential trend, which does not capture the data satisfactorily (Fig. 1b). Note that we impose $\mathcal{U}(n, t) = 0$ here. If $\mathcal{U}(n, t) \neq 0$, we can obtain a bounded solution similar to Eq. 2 subject to $\mathcal{C} \left(\frac{(2\ell-1)\pi}{2N} \right)^2 \geq -(\mathcal{U}/N)$ [45], and thus a similar truncated power-law trend for $S(t)$. Some results for non-zero $\mathcal{U}(n, t)$ obtained using monte-carlo simulations have been discussed elsewhere [31]. Truncated power-law interaction lifetimes have been observed in a variety of biological and bio-derived systems, such as protein-DNA (or RNA) strand interactions, protein-protein interactions, and biomolecule-coated microspheres [28–30, 32, 46–48]. This suggests that sequential multi-step binding-unbinding interactions may be more prevalent across biological contexts than previously appreciated. Nevertheless, the former does not imply that the power-law behavior is universal for all types of proteins [49]. Therefore, a thorough validation and calibration of N and \mathcal{C} for different protein types would require studying their interactions through controlled experiments [50–54] or computationally expensive all-atom MD simulations [55, 56].

This is beyond the scope of the present work and merits further attention.

As the interaction specificity is hidden in the binding-unbinding pathways, we now test the model for two types of specific interactions: interactions via multi-step sequential binding-unbinding ($N > 1$) and single-step binding-unbinding ($N = 1$). We examine whether these interaction types influence condensate dynamics. It is interesting that despite of the same mean lifetime τ_m , these two mechanisms result in distinct lifetime distributions (Fig. 1c). Both distributions indicate that short and long lifetimes are probable. Though the probability of short lifetimes is higher for $N > 1$ than that of $N = 1$, the fat-tail in the distribution with low probabilities for $N > 1$ serves to complement the mean lifetime (see SI section SI1 and Fig. S1).

To examine condensate dynamics, we integrate the above model with Brownian dynamics simulation in a hybrid manner. The molecules and clusters are allowed to diffuse. When two molecules (whether part of clusters or individuals) are in close proximity, they bind with a sticking probability p_s . Each molecule has a certain number of binding regions, represented by n_b . The molecules remain bound for a lifetime that is randomly drawn from the PDFs shown in Fig. 1c, followed by unbinding. This is how cluster formation, growth, aggregation, fragmentation, and dissolution can occur in the present system. Here, we ignore the hydrodynamic interactions among individual protein molecules and phase-separated clusters that perform the Brownian motion. The simulation details are described in SI section SI2.

Results—We define the average size $\langle A \rangle$ and total number of clusters $\langle N_A \rangle$ following the definition of Vicsek [57, 58]: $\langle A \rangle = (\sum_{A \geq 2} n_A A^2) / (\sum_{A \geq 2} n_A A)$ and $\langle N_A \rangle = \sum_{A \geq 2} n_A$, where n_A is the number of clusters of size A , and A is the two-dimensional volume of a cluster scaled by the nominal two-dimensional volume a_p . Without loss of generality, a_p is set to 1. Unless specified, the error bars in the results represent the 95% confidence limits from four independent simulations.

The growth of $\langle A \rangle$ over time shows diffusion-limited aggregation in the early stage of phase separation (Fig. 2a and SI Fig. S2a). In this period, the variation of $\langle N_A \rangle$ with time shows a linear trend on the log-log scale (Fig. 2b and SI Fig. S2b). It is evident that molecular collisions via diffusion is one of the prerequisites for cluster formation, growth, and aggregation. We could have expected reaction-limited growth if the binding kinetics (incorporated as the sticking probability p_s in the model) had been much slower than diffusion, implying the requirement of numerous collisional contacts before a successful binding event [58, 59]. Family et al. [58] showed that cluster aggregation is chemically controlled and reaction-limited if $p_s \ll 0.1$. However, the present study employs $p_s = 0.1$ and therefore we can expect diffusion-limited growth, consistent with the findings of Family et al. [58].

Considering the pure growth process, if the coarsening

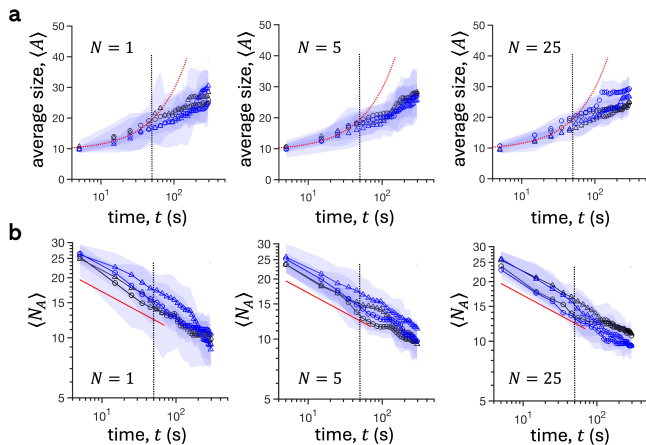


FIG. 2. Variation of the average size of clusters $\langle A \rangle$ (a) and the total number of clusters $\langle N_A \rangle$ (b) with time t for different values of the total number of probable conformational changes N . Here, the black and blue symbols are for the number of binding regions $n_b = 3$ and $n_b = 4$, respectively, and \circ and \triangle represent the mean lifetime of the lifetime distribution $\tau_m = 15$ s and $\tau_m = 130$ s, respectively. Panels in (a) and (b) correspond to the area fraction $a_f = 0.1$. The red dotted curves in panel (a) fit the data points by $y = mx + c$ on the left of the black dotted vertical lines, and the red solid lines in panel (b) represent the slope -0.2 . The shaded regions represent the 95% confidence limits from four independent simulations.

dynamics of molecules or a population of clusters undergoing Brownian motion follows the Smoluchowski coagulation dynamics, then it can be shown that $\langle A \rangle \propto t$ in absence of hydrodynamics interactions [9, 11, 60–63]. This scaling is reflected in Fig. 2a and *SI Fig. S2a*, irrespective of the ranges of parameters. However, the coarsening dynamics deviates from this scaling in the long-time limit. Interestingly, it can be noted that in the variation of $\langle N_A \rangle$ with time, there are minute oscillations of very small amplitudes and large wavelengths in the long time limit (Fig. 2b and *SI Fig. S2b*). This is an indication of aggregation-fragmentation processes [64]. The fragmentation process is equivalent to the unbinding events. In that case, the growth dynamics does not necessarily need to follow the same scaling as in diffusion-limited growth in the long-time limit. The findings of simultaneous growth, aggregation, and fragmentation collectively deduce that clusters are dynamic, and they can participate in neighbor exchange events.

A schematic illustrating the different modes of neighbor exchange is shown in Fig. 3a. We define a new quantity: the cumulative number of neighbor exchanges N_{ex}^c (see *SI section SI3* for how we obtain N_{ex}^c). The cumulative total number of neighbor exchange events N_{ex}^c with time has been observed to be strongly influenced by the specificity in the binding-unbinding interactions of protein molecules (Fig. 3b,c) for the case of the same mean lifetime τ_m . In Fig. 3b,c, the dynamic behavior changes significantly with the total number of probable conforma-

tional changes N and the number of binding regions n_b . Compared to the case for single-step binding-unbinding ($N = 1$), N_{ex}^c is higher for interactions via multi-step sequential binding-unbinding corresponding to $N > 1$. Recall that when two lifetime distributions of the same mean lifetime τ_m are compared for $N = 1$ and $N > 1$, the probability of very short lifetimes is higher and the probability of intermediate lifetimes is lower for $N > 1$ (Fig. 1c and *SI Fig. S1*). This is why, a higher number of exchange events is expected for cases $N > 1$ during the early stage of phase separation. With an increase in N and a decrease in n_b , N_{ex}^c increases (Fig. 3b,c), highlighting the roles of both N and n_b in driving the specificity in protein interactions.

As the mean lifetime $\tau_m = 130$ s is comparable to the total duration of the simulations (see Fig. 3b,c), it might initially appear that N_{ex}^c would continue to increase with time. However, a closer look at the trends reveals the following interesting insight. The trends for cases $N > 1$ show the scaling $N_{ex}^c \propto t^{1/2}$, whereas for $N = 1$, $N_{ex}^c \propto t$. If these trends persist, it implies that in time $t \gg \tau_m$, N_{ex}^c would tend to saturate for $N > 1$, but N_{ex}^c would continue to increase for $N = 1$. Therefore, a crossover between $N = 1$ and $N > 1$ would be expected in time $t \gg \tau_m$. This is indeed the case when τ_m is reduced to 15 s, which is much smaller than the total duration of the simulations; the crossover is noticeable in the long-time limit in Fig. 3d,e.

The findings in Fig. 3 reveal that one of the systems undergoes aging through a gradual decrease in the frequency of exchange events, particularly when binding-unbinding interactions are a multi-step sequential process. Interestingly, for the same mean lifetime τ_m , one mechanism (sequential multi-step binding-unbinding) leads to aging, while another (single-step mechanism) does not, indicating a possible connection between aging and changes in protein interactions. The aging of condensates has previously been observed in experiments [5, 13]. It has been speculated that a time-dependent evolution in the strength and specificity of the interaction may lead to aging [5]. As condensates age, protein interaction lifetimes are expected to increase, hence reducing fluidity of the clusters and driving a transition from a liquid-like to a gel-like state.

It is important to note that the prolonged lifetimes can arise from multi-step sequential binding and unbinding interactions when $N > 1$ (see Fig. 1c and *SI Fig. S1*). This scenario can be visualized as two protein molecules sequentially binding to one another, becoming trapped in a conformational state as $n \rightarrow N$ (see Fig. 1a). The protein molecules then would probably take longer time to return to the unbound state before participating in exchange events. This trapping mechanism is analogous to the continuous-time random-walk trap model described by Bouchaud [65, 66]. Recently, similar trap models have been developed to explain the rheology of aging condensates [67, 68].

The reasoning for the scalings in Fig. 3, $N_{ex}^c \propto t$ for

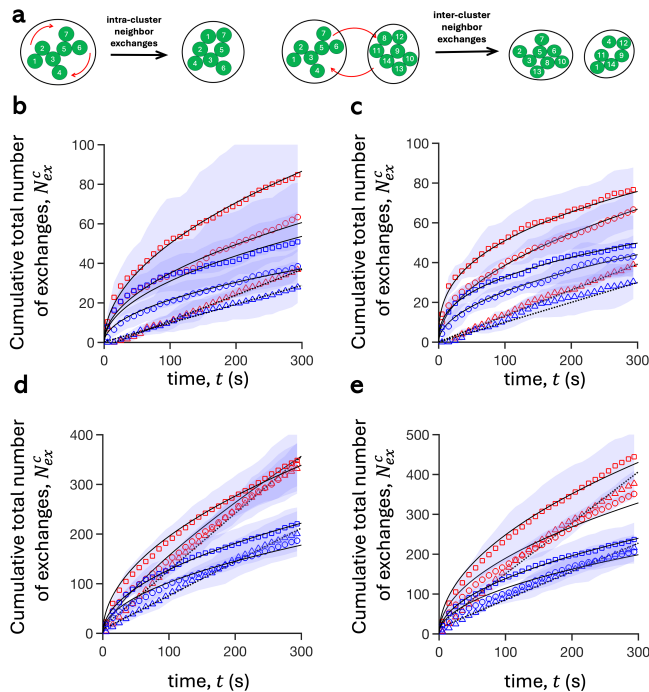


FIG. 3. (a) Schematic of different types of neighbor exchanges. Variation of the cumulative total number of exchanges N_{ex}^c with time t . Parameters: (b) area fraction $a_f = 0.05$, the mean lifetime of distribution $\tau_m = 130$ s; (c) $a_f = 0.1$, $\tau_m = 130$ s; (d) $a_f = 0.05$, $\tau_m = 15$ s; (e) $a_f = 0.1$, $\tau_m = 15$ s. In (b)–(e), red and blue symbols correspond to the number of binding regions $n_b = 3$ and $n_b = 4$, respectively. Here, \triangle , \circ , and \square are for the total number of probable conformational changes $N = 1$, $N = 5$, and $N = 25$, respectively. The black solid curves are fit for $y = mx^{1/2}$ and black dotted lines for $y = mx$. The shaded regions represent the 95% confidence limits from four independent simulations.

$N = 1$ and $N_{ex}^c \propto t^{1/2}$ for $N > 1$, is as follows. If the time intervals between successive neighbor exchange events are exponentially distributed (see Fig. 1c), as in a Poisson process with a mean waiting time τ_m , the number of jumps within time t would be scaled as $\sim t/\tau_m$. Therefore, $N_{ex}^c \propto t$ is expected for the case $N = 1$. But, if there are traps in the jump process, leading to prolonged waiting times, the distribution of jump times would be a heavy-tailed power-law with exponent α . The former is similar to the continuous-time random-walk trap model [66]. Then the number of jumps within time t would be scaled as $\sim t^\alpha$. The value of α is $1/2$ for Lévy distribution which is an outcome of a limiting case $N \rightarrow \infty$. Therefore, we can expect the scaling $N_{ex}^c \propto t^{1/2}$ for cases $N > 1$. In essence, without further modifications, the same model demonstrates its strength in capturing both the aging of protein interactions and its impact on the exchange dynamics.

Motivated by these insights, another important aspect that arises is whether the different types of protein interaction and exchange dynamics can also influence the size

distribution of condensates. This topic is of great importance, as it can reveal a connection between an alteration in the size distribution of condensates and the onset of disease progression or recovery [2, 5, 69, 70]. It is well-understood that different merging/coalescence dynamics can impact the size distribution of phase-separated droplets. A recent work proposed a mechanism on how nucleation and preferential merging can lead to different size distributions [8]. In the former, the role of protein interactions has not been considered explicitly, although some connections can be anticipated between protein-specific interaction leading to preferential merging. It remains unclear whether the specific interaction mechanisms between individual protein molecules impact the size distribution, in addition to other factors such as variability in the nucleation rate and merging dynamics.

Extending this line of thought, recall that we use the sticking probability, which accounts for the same nucleation and merging mechanism of individual molecules and clusters (see *SI* section SI2). The merging mechanism would be complicated if there were hydrodynamic interactions [11, 12, 61, 62]. Our model and simulation approach allow us to isolate all other factors and focus specifically on the dependence of the size distributions on the specific interaction mechanisms.

When the complementary cumulative distribution function (CCDF), where $\text{CCDF} = 1 - \int_0^A f(A', t) dA'$ and $f(A', t)$ is the probability density of size A' at time t , is plotted with the scaled size of clusters $A/\langle A \rangle$ on the log-log scale, two distinct trends emerge for cases $N = 1$ and $N > 1$ (Fig. 4). For $N > 1$, the curvature in the trends is clearly visible, while the trends are linear for $N = 1$. The fits in Fig. 4 represent a transition in the distribution from the power-law to the truncated power-law as the binding-unbinding process shifts from a single-step pathway to a sequential multi-step pathway. Power-law and truncated power-law distributions have been previously reported in experiments [7, 8], which are specific to different types of proteins. An exponential distribution has been observed in a synthetic Corelet system [8]. Our model does not capture the transition from a truncated power-law to a pure exponential distribution for the ranges of parameters examined here.

The total simulation time in the present work is very small ($t = 300$ s) compared to other relevant time scales (say, hours and days). In addition, our simulation box size and number of molecules simulated are also smaller compared to the size of a nucleus. At present, it is beyond the scope of the simulation to investigate a large system for a much longer period. Although more work may be required to claim the connection between size distribution and protein-specific interactions, the change in trends is distinguishable in Fig. 4 for $N = 1$ and $N > 1$. Therefore, rather than drawing a definitive conclusion, we state that the current findings point toward a possible connection between changes in the size distribution of biomolecular condensates and alterations in the interaction pathways (changes in N , and potentially $\mathcal{C}(n, t)$

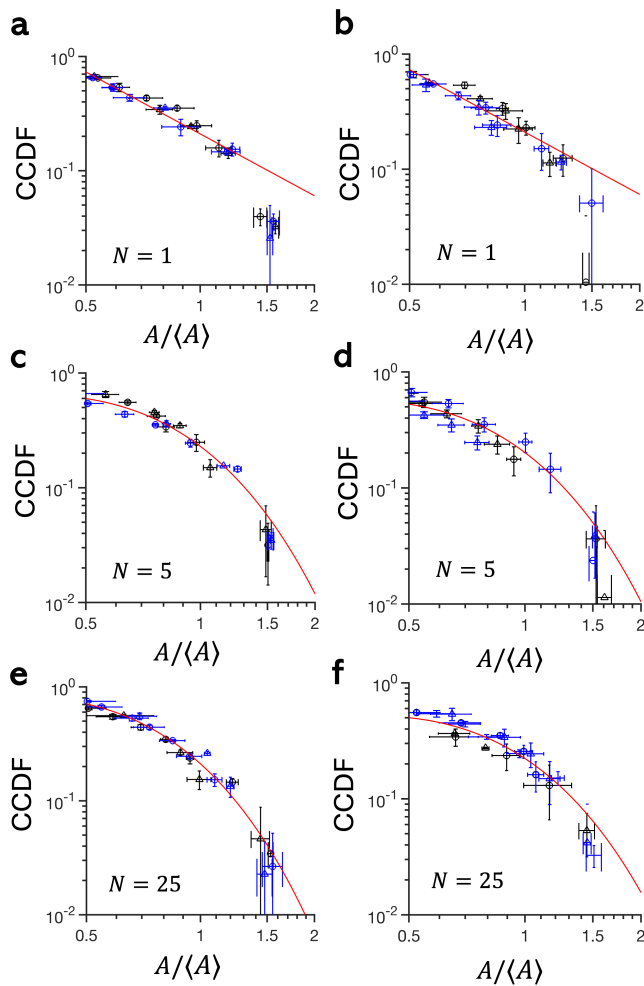


FIG. 4. After $t = 300$ s of simulation, the complementary cumulative distribution functions (CCDF) of the scaled size $A/\langle A \rangle$ of the clusters are shown in log-log scale: (a), (c), and (e) are for the area fraction $a_f = 0.05$, and (b), (d), and (f) are for $a_f = 0.1$. Here, the black and blue symbols are for the number of binding regions $n_b = 3$ and $n_b = 4$, respectively, and \circ and \triangle represent the mean lifetime of the lifetime distribution $\tau_m = 15$ s and $\tau_m = 130$ s, respectively. The red lines in (a) and (b) are fit for $y = mx^\alpha$, and the red curves in (c)–(f) for $y = a \exp(-bx)x^\beta$. The error bars represent the 95% confidence limits from four independent simulations.

or $U(n, t)$). An alteration in the size distribution of condensates is in-turn indicative of various aging, anti-aging processes, or the progression and regression of a disease. Thus, the multi-step binding-unbinding interaction pathway explored here can be a key to connecting protein structural changes to condensate dynamics and functions associated with key biological processes [23, 71].

Discussions—The specificity of protein interaction required for the formation of protein-specific condensates in a crowded and heterogeneous cellular environment may at times seem at odds with the fluidic nature and dynamic features of the condensates. Explanations of

fluidity and exchange of molecules between the condensed (dense) and bulk (dilute) phases usually involve a tight control of the condensing protein concentration just above the saturation concentration (C_{sat}), or the introduction of biochemical or biomechanical activity within the condensates to supply the energy needed to rapidly breakdown the strong interactions. Intuitively, the activity-driven fluidization of condensates appears to be a much more likely explanation than a strict population control of interacting proteins within biological systems.

In the present work, we propose an alternative protein interaction mechanism that can capture both the formation of protein-specific condensates and their fluidic nature altogether. A possible explanation lies in the specificity of the binding-unbinding interaction mechanisms leading to distinct interaction lifetime distributions. Particularly, two interaction lifetime distributions emerge when binding-unbinding follows a single-step or a sequential multi-step process, where the former leads to the exponential distribution and the latter to the non-exponential truncated power-law distribution. Most instances where truncated powerlaw lifetime distributions have been observed in experimental systems in the past, the origin has been attributed to the existence of multiple interacting populations, each with their own unique exponential distribution. However, recently, it has been shown by us and others that such a lifetime distribution can arise within single populations of interacting proteins as well, when the binding-unbinding process follows a multistep sequential process. We have shown here that such a sequential process can lead to non-exponential interaction lifetime distributions as a function of the number of steps within the process, as well as the mobility of the protein across these quasistable bound conformations, and the energy barriers separating consequent conformational states. Further, integrating the model with Brownian dynamics simulations, we demonstrate how questioning the lifetime distributions of individual protein-protein interactions can potentially explain the important features of condensates, for example, their fluidic nature, how aging in protein interactions can influence the exchange dynamics, and the size distribution of condensates.

Our model, without any further modification, also highlights a possible link between biological aging and changes in the size distribution of condensates, which can be attributed to minor structural changes in protein interactions [5, 38, 71]. A notable observation is that, apart from different nucleation mechanisms and merging dynamics, only the changes in the interaction lifetime distributions without affecting the specificity of interactions (as measured by mean interaction lifetimes) are an important factor affecting the physical properties of biomolecular condensates. This observation underscores the need to dig deeper into factors such as ‘high interaction specificity and low conformational heterogeneity’ as described by Hess & Joseph [23], and how together

they influence interaction lifetimes and the biophysics of condensates. It also makes us curious to examine how sequential binding-unbinding-based specific interactions leading to non-exponential interaction lifetimes between biomolecular species might influence other biological processes, such as enzyme cascades [72, 73] and molecular communication networks [74].

It is important to mention that the present modeling framework needs more refinement to incorporate electrostatic and other long-range interactions, including hydrodynamic interactions among Brownian droplets and individual molecules. Other important factors that require

consideration are reaction-dependent non-equilibrium active processes and diffusiophoretic activity, which can modify the diffusivity of the Brownian droplets. These are the directions for advancements and form part of future work.

ACKNOWLEDGMENTS

We acknowledge funding support from US Army Research Office grants W911NF-23-1-0329, W911NF-22-1-0047, and San Diego State University Research Foundation.

-
- [1] A. Hyman, C. Weber, and F. Jülicher, Liquid-liquid phase separation in biology, *Ann. Rev. Cell Dev. Biol.* **30**, 39 (2014).
- [2] Y. Shin and C. Brangwynne, Liquid phase condensation in cell physiology and disease, *Science* **357**, eaaf4382 (2017).
- [3] S. Banani, H. Lee, A. Hyman, and M. Rosen, Biomolecular condensates: organizers of cellular biochemistry, *Nat. Rev. Mol. Cell Biol.* **18**, 285 (2017).
- [4] C. Brangwynne, C. Eckmann, D. Courson, A. Rybarska, C. Hoeghe, J. Gharakhani, F. Jülicher, and A. Hyman, Germline p granules are liquid droplets that localize by controlled dissolution/condensation, *Science* **324**, 1729 (2009).
- [5] A. Patel, H. Lee, L. Jawerth, S. Maharana, *et al.*, A liquid-to-solid phase transition of the als protein fus accelerated by disease mutation, *Cell* **162**, 1066 (2015).
- [6] S. Banani, A. Rice, W. Peeples, Y. Lin, S. Jain, R. Parker, and M. Rosen, Compositional control of phase-separated cellular bodies, *Cell* **166**, 651 (2016).
- [7] C. Caragine, S. Haley, and A. Zidovska, Nucleolar dynamics and interactions with nucleoplasm in living cells, *Elife* **8**, e47533 (2019).
- [8] D. Lee, C. Choi, D. Sanders, L. Beckers, J. Riback, C. Brangwynne, and N. Wingreen, Size distributions of intracellular condensates reflect competition between coalescence and nucleation, *Nat. Phys.* **19**, 586 (2023).
- [9] E. D. Siggia, Late stages of spinodal decomposition in binary mixtures, *Phys. Rev. A* **20**, 595 (1979).
- [10] H. Tanaka, A new coarsening mechanism of droplet spinodal decomposition, *J. Chem. Phys.* **103**, 2361 (1995).
- [11] H. Tanaka, Viscoelastic phase separation, *Journal of Physics: Condensed Matter* **12**, R207 (2000).
- [12] R. Shimizu and H. Tanaka, A novel coarsening mechanism of droplets in immiscible fluid mixtures, *Nat. Commun.* **6**, 7407 (2015).
- [13] L. Jawerth, E. Fischer-Friedrich, S. Saha, *et al.*, Protein condensates as aging maxwell fluids, *Science* **370**, 1317 (2020).
- [14] A. Vidal Ceballos, J. Díaz A, J. Preston, C. Vairamon, C. Shen, R. Koder, and S. Elbaum-Garfinkle, Liquid to solid transition of elastin condensates, *Proc. Nat. Acad. Sci.* **119**, e2202240119 (2022).
- [15] M. Poudyal, K. Patel, L. Gadhe, A. Sawner, S. Maiti, *et al.*, Intermolecular interactions underlie protein/peptide phase separation irrespective of sequence and structure at crowded milieu, *Nat. Commun.* **14**, 6199 (2023).
- [16] L. Emmanouilidis, E. Bartalucci, Y. Kan, M. Ijavi, M. Pérez, P. Afanasyev, D. Boehringer, J. Zehnder, S. Parekh, M. Bonn, *et al.*, A solid beta-sheet structure is formed at the surface of fus droplets during aging, *Nat. Chem. Biol.* **20**, 1044 (2024).
- [17] G. Benedek, Cataract as a protein condensation disease: the proctor lecture., *Investigative ophthalmology & visual science* **38**, 1911 (1997).
- [18] S. Mehra, S. Sahay, and S. Maji, α -synuclein misfolding and aggregation: Implications in parkinson's disease pathogenesis, *Biochimica et Biophysica Acta (BBA)-Proteins and Proteomics* **1867**, 890 (2019).
- [19] S. Ray, N. Singh, R. Kumar, K. Patel, S. Pandey, D. Datta, *et al.*, α -synuclein aggregation nucleates through liquid-liquid phase separation, *Nat. Chemistry* **12**, 705 (2020).
- [20] C. Brangwynne, P. Tompa, and R. Pappu, Polymer physics of intracellular phase transitions, *Nat. Phys.* **11**, 899 (2015).
- [21] J. Choi, A. Holehouse, and R. Pappu, Physical principles underlying the complex biology of intracellular phase transitions, *Ann. Rev. Biophys.* **49**, 107 (2020).
- [22] Y. Zhang, B. Xu, B. Weiner, Y. Meir, and N. Wingreen, Decoding the physical principles of two-component biomolecular phase separation, *Elife* **10**, e62403 (2021).
- [23] N. Hess and J. Joseph, Structured protein domains enter the spotlight: modulators of biomolecular condensate form and function, *Trends in Biochemical Sciences* (2025).
- [24] P. Katira, A. Agarwal, and H. Hess, A random sequential adsorption model for protein adsorption to surfaces functionalized with poly (ethylene oxide), *Adv. Mater.* **21**, 1599 (2009).
- [25] J. Changeux and S. Edelstein, Conformational selection or induced fit? 50 years of debate resolved, *F1000 Biology Rep.* **3**, 19 (2011).
- [26] M. Seo, J. Park, E. Kim, S. Hohng, and H. Kim, Protein conformational dynamics dictate the binding affinity for a ligand, *Nat. Commun.* **5**, 3724 (2014).
- [27] A. Stank, D. Kokh, J. Fuller, and R. Wade, Protein binding pocket dynamics, *Acc. Chem. Res.* **49**, 809 (2016).
- [28] P. Biancaniello, A. Kim, and J. Crocker, Colloidal inter-

- actions and self-assembly using dna hybridization, *Phys. Rev. Lett.* **94**, 058302 (2005).
- [29] W. Rogers, T. Sinno, and J. Crocker, Kinetics and non-exponential binding of dna-coated colloids, *Soft Matter* **9**, 6412 (2013).
- [30] M. Penna, M. Mijajlovic, and M. Biggs, Molecular-level understanding of protein adsorption at the interface between water and a strongly interacting uncharged solid surface, *J. Am. Chem. Soc.* **136**, 5323 (2014).
- [31] M. Armstrong, J. Rodriguez III, P. Dahl, P. Salamon, H. Hess, and P. Katira, Power law behavior in protein desorption kinetics originating from sequential binding and unbinding, *Langmuir* **36**, 13527 (2020).
- [32] D. Garcia, G. Fettweis, D. Presman, V. Paakinaho, C. Jarzynski, A. Upadhyaya, and G. Hager, Power-law behavior of transcription factor dynamics at the single-molecule level implies a continuum affinity model, *Nucleic Acids Res.* **49**, 6605 (2021).
- [33] Z. Chen, S. Boyken, M. Jia, F. Busch, D. Flores-Solis, M. Bick, P. Lu, *et al.*, Programmable design of orthogonal protein heterodimers, *Nature* **565**, 106 (2019).
- [34] M. Rubinstein and A. Dobrynin, Solutions of associative polymers, *Trends in Polymer Sci.* **5**, 181 (1997).
- [35] A. Semenov and M. Rubinstein, Thermoreversible gelation in solutions of associative polymers. 1. statics, *Macromolecules* **31**, 1373 (1998).
- [36] Y. Zhang, A. Pyo, R. Kliegman, Y. Jiang, C. Brangwynne, H. Stone, and N. Wingreen, The exchange dynamics of biomolecular condensates, *Elife* **12**, RP91680 (2024).
- [37] S. Biswas and D. Potoyan, Molecular drivers of aging in biomolecular condensates: Desolvation, rigidification, and sticker lifetimes, *PRX life* **2**, 023011 (2024).
- [38] A. Garaizar, J. Espinosa, J. Joseph, G. Krainer, Y. Shen, T. Knowles, and R. Collepardo-Guevara, Aging can transform single-component protein condensates into multiphase architectures, *Proc. Nat. Acad. Sci.* **119**, e2119800119 (2022).
- [39] D. Baker, What has de novo protein design taught us about protein folding and biophysics?, *Protein Science* **28**, 678 (2019).
- [40] H. Lu, Probing single-molecule protein conformational dynamics, *Acc. Chem. Res.* **38**, 557 (2005).
- [41] J. Guo and H. Zhou, Protein allostery and conformational dynamics, *Chem. Rev.* **116**, 6503 (2016).
- [42] C. Brooks III, J. Onuchic, and D. Wales, Taking a walk on a landscape, *Science* **293**, 612 (2001).
- [43] D. Wales and T. Bogdan, Potential energy and free energy landscapes, *J. Phys. Chem. B* **110**, 20765 (2006).
- [44] J. Joseph, K. Röder, D. Chakraborty, R. Mantell, and D. Wales, Exploring biomolecular energy landscapes, *Chem. Commun.* **53**, 6974 (2017).
- [45] V. Zaitsev and A. Polyanin, *Handbook of exact solutions for ordinary differential equations* (2002).
- [46] M. Mazzocca, E. Colombo, A. Callegari, and D. Mazza, Transcription factor binding kinetics and transcriptional bursting: What do we really know?, *Current Opinion in Structural Biology* **71**, 239 (2021).
- [47] M. Elkins, A. Bandara, G. Pantelopulos, J. Straub, and M. Hong, Direct observation of cholesterol dimers and tetramers in lipid bilayers, *J. Phys. Chem. B* **125**, 1825 (2021).
- [48] K. Lyu, H. Chen, J. Gao, J. Jin, H. Shi, D. Schwartz, and D. Wang, Protein desorption kinetics depends on the timescale of observation, *Biomacromolecules* **23**, 4709 (2022).
- [49] S. Kulin, R. Kishore, J. Hubbard, and K. Helmersson, Real-time measurement of spontaneous antigen-antibody dissociation, *Biophys. J.* **83**, 1965 (2002).
- [50] J. Gebhardt, D. Suter, R. Roy, Z. Zhao, A. Chapman, S. Basu, T. Maniatis, and X. Xie, Single-molecule imaging of transcription factor binding to dna in live mammalian cells, *Nat. Methods* **10**, 421 (2013).
- [51] S. Banerjee, S. Maurya, and R. Roy, Single-molecule fluorescence imaging: Generating insights into molecular interactions in virology, *J. Biosciences* **43**, 519 (2018).
- [52] M. Bernalova, S. Mahanta, and M. Krishnan, Single-molecule trapping and measurement in solution, *Curr. Opinion Chem. Biol.* **51**, 113 (2019).
- [53] M. Bernalova, R. Oz, F. Westerlund, and M. Krishnan, Single-molecule trapping and measurement in a nanostructured lipid bilayer system, *Langmuir* **38**, 13923 (2022).
- [54] R. Walker-Gibbons, X. Zhu, A. Behjatian, T. Bennett, and M. Krishnan, Sensing the structural and conformational properties of single-stranded nucleic acids using electrometry and molecular simulations, *Sci. Rep.* **14**, 20582 (2024).
- [55] E. Henry, R. Best, and W. Eaton, Comparing a simple theoretical model for protein folding with all-atom molecular dynamics simulations, *Proc. Nat. Acad. Sci.* **110**, 17880 (2013).
- [56] A. Dommer, N. Wauer, S. Marrink, and R. Amaro, All-atom virus simulations to tackle airborne disease, *Curr. Op. Struct. Biol.* **92**, 103048 (2025).
- [57] T. Vicsek and F. Family, Dynamic scaling for aggregation of clusters, *Phys. Rev. Lett.* **52**, 1669 (1984).
- [58] F. Family, P. Meakin, and T. Vicsek, Cluster size distribution in chemically controlled cluster-cluster aggregation, *J. Chem. Phys.* **83**, 4144 (1985).
- [59] M. Lin, H. Lindsay, D. Weitz, R. Ball, R. Klein, and P. Meakin, Universal reaction-limited colloid aggregation, *Phys. Rev. A* **41**, 2005 (1990).
- [60] S. Chandrasekhar, Stochastic problems in physics and astronomy, *Rev. Mod. Phys.* **15**, 1 (1943).
- [61] V. Kumaran, Droplet interaction in the spinodal decomposition of a fluid, *J. Chem. Phys.* **109**, 7644 (1998).
- [62] V. Kumaran, Effect of convective transport on droplet spinodal decomposition in fluids, *J. Chem. Phys.* **109**, 2437 (1998).
- [63] F. Chen, W. Guo, and H. Shum, Fractal-dependent growth of solidlike condensates, *Phys. Rev. Lett.* **133**, 118401 (2024).
- [64] N. Brilliantov, W. Otieno, S. Matveev, A. Smirnov, E. Tyrtshnikov, and P. Krapivsky, Steady oscillations in aggregation-fragmentation processes, *Phys. Rev. E* **98**, 012109 (2018).
- [65] J. Bouchaud, Weak ergodicity breaking and aging in disordered systems, *Journal de Physique I* **2**, 1705 (1992).
- [66] C. Monthus and J. Bouchaud, Models of traps and glass phenomenology, *Journal of Physics A: Mathematical and General* **29**, 3847 (1996).
- [67] J. Lin, Modeling the aging of protein condensates, *Phys. Rev. Res.* **4**, L022012 (2022).
- [68] R. Takaki, L. Jawerth, M. Popović, and F. Jülicher, Theory of rheology and aging of protein condensates, *PRX Life* **1**, 013006 (2023).
- [69] A. Molliex, J. Temirov, J. Lee, M. Coughlin, A. Kana-

- garaj, H. Kim, T. Mittag, and J. Taylor, Phase separation by low complexity domains promotes stress granule assembly and drives pathological fibrillization, *Cell* **163**, 123 (2015).
- [70] A. Buchwalter and M. Hetzer, Nucleolar expansion and elevated protein translation in premature aging, *Nat. Commun.* **8**, 1 (2017).
- [71] M. Linsenmeier, M. Hondele, F. Grigolato, E. Secchi, K. Weis, and P. Arosio, Dynamic arrest and aging of biomolecular condensates are modulated by low-complexity domains, rna and biochemical activity, *Nat. Commun.* **13**, 3030 (2022).
- [72] Y. Zhang and H. Hess, Toward rational design of high-efficiency enzyme cascades, *ACS Catalysis* **7**, 6018 (2017).
- [73] X. Zhao, H. Palacci, V. Yadav, M. Spiering, M. Gilson, P. Butler, H. Hess, S. Benkovic, and A. Sen, Substrate-driven chemotactic assembly in an enzyme cascade, *Nature Chemistry* **10**, 311 (2018).
- [74] T. Nakano, M. Moore, F. Wei, A. Vasilakos, and J. Shuai, Molecular communication and networking: Opportunities and challenges, *IEEE transactions on nanobioscience* **11**, 135 (2012).

Sequential binding-unbinding based specific interactions highlight exchange dynamics and size distribution of condensates: Supplementary Information

Bhanjan Debnath¹ and Parag Katira¹

¹*Department of Mechanical Engineering, San Diego State University, CA, 92182, USA*

Supplementary Information (SI)

SI1 Lifetime distributions from sequential binding-unbinding based model

Consider the case with a uniform energy landscape for sequential binding and unbinding. Therefore, neglecting the drift and treating \mathcal{C} as a constant, the system is represented by

$$\frac{\partial \mathcal{P}(n, t)}{\partial t} = \mathcal{C} \frac{\partial}{\partial n} \left[\frac{\partial \mathcal{P}(n, t)}{\partial n} \right]. \quad (\text{S1})$$

We assume that $n = 0$ state is an unbound state. While binding and unbinding, the first conformation bound state is represented by $n = 1$. A total number of probable conformation changes that can occur during sequential binding and unbinding is $n = N$. To solve S1, we use $n = 0$ and $n = N$ as absorbing and reflective boundaries,

respectively. Hence, the boundary conditions used to solve Eq. S1 are

$$\mathcal{P}(n = 0, t) = 0 \quad (\text{S2})$$

$$\frac{\partial \mathcal{P}}{\partial n}(n = N, t) = 0 \quad (\text{S3})$$

We use the following as an initial condition as $n = 1$ would be the first bound state

$$\begin{aligned} \mathcal{P}(n, t = 0) &= \delta(n - 1) \\ \delta(n - 1) &= 0 \text{ for all } n \text{ except } n = 1 \end{aligned} \quad (\text{S4})$$

which satisfies $\int \mathcal{P} dn = \int \delta(n - 1) dn = 1$. Although conformational bound states are represented by discrete whole numbers $\mathcal{W} = \{0, 1, 2, 3, 4, 5, \dots\}$, we solve the above system by treating it as a continuum. An exact solution is possible for the above system [1, 2],

$$\begin{aligned} \mathcal{P}(n, t) = \frac{2}{N} \sum_{\ell=1}^{\infty} \left\{ \sin \left[\frac{(2\ell - 1)\pi}{2N} \right] \sin \left[\frac{(2\ell - 1)\pi}{2N} n \right] \right. \\ \left. \times \exp \left[- \mathcal{C} \left(\frac{(2\ell - 1)\pi}{2N} \right)^2 t \right] \right\} \end{aligned} \quad (\text{S5})$$

Next, the survival probability, which is defined as $S(t) = \int_{n=0}^{n=N} \mathcal{P}(n, t) dn$, is

$$\begin{aligned} S(t) = \frac{4}{\pi} \sum_{\ell=1}^{\infty} \left\{ \frac{1}{(2\ell - 1)} \sin \left[\frac{(2\ell - 1)\pi}{2N} \right] \right. \\ \left. \times \exp \left[- \mathcal{C} \left(\frac{(2\ell - 1)\pi}{2N} \right)^2 t \right] \right\}. \end{aligned} \quad (\text{S6})$$

The probability distribution of lifetime can be obtained as PDF = $\mathcal{F}(t_i) = -dS(t)/dt$. We obtain the lifetimes of the interaction t_i by taking the inverse, i.e., $t_i = \mathcal{F}^{-1}(\text{PDF})$, and the mean of t_i is represented by the mean lifetime t_m .

For different values of N , the PDFs (probability distribution function) are shown

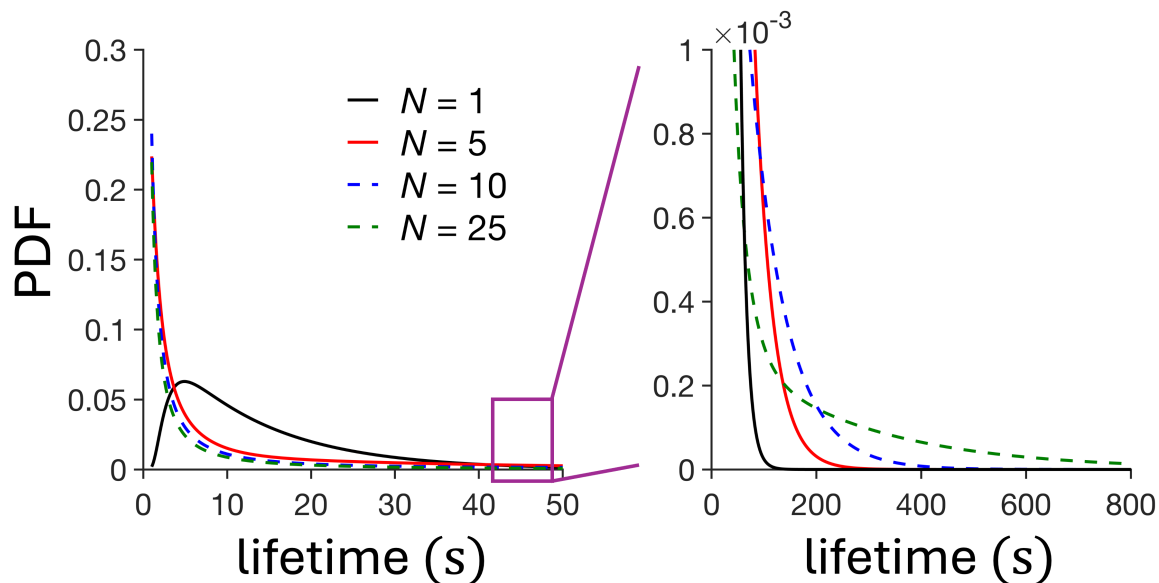


Figure S1: The PDFs (probability distribution function) of lifetimes for different values of N . The mean lifetime t_m is set to ~ 15 s. The values of \tilde{C} are 0.034, 0.3, 0.6, and 1 for $N = 1, 5, 10,$ and 25 , respectively. Here, $\tilde{C} = C/\alpha$ and α represents a square unit of conformation changes per second

in the first panel of Fig. S1, keeping the mean lifetime t_m the same. Except for the exponential trend in $N = 1$, the rest of the trends are power-law for $N > 1$. In the long time limit, the exponential trend in $N = 1$ decays much faster than $N > 1$. As N increases, the decay is slower (see the enlarged second panel in Fig. S1). The fat-tails in the long time limit for $N > 1$ complement the mean lifetime t_m (the second panel in Fig. S1), however, the probability of significantly large lifetimes is extremely low, irrespective of N .

Using the form $S(t)$ in Eq. S6 for $N = 1$ may be inappropriate, as it implies only one conformation state and the continuum limit is invalid. Note that $N = 1$ is equivalent to the first-order kinetics, which must reflect an exponential trend. Surprisingly, the form $S(t)$ in Eq. S6 predicts an exponential trend for $N = 1$ and thus similar exponential trend by $\text{PDF} = -dS(t)/dt$ (Fig. S1). Therefore, whether we use Eq. S6 for $N = 1$ or an exponential distribution function, the outcome remains the same.

SI2 Hybrid simulation method

We use the Brownian dynamics (BD) to simulate the Brownian motion of individual molecules and their phase-separated clusters in a two-dimensional square box using periodic boundary conditions in both the x - and y - directions. The coarse-grained protein molecules are treated as non-overlapping circular discs of radius $r_p = 5$ nm, and their motion is simulated using the Cichocki–Hinsen algorithm [3, 4]. This chosen size of a molecule is not specific to any protein. Some miRNA proteins was previously reported to have a similar size range [5]. For simplicity, we ignore all potential interactions among molecules. The electrostatic, other long-range, and hydrodynamic interactions among molecules and clusters are ignored. The simulation time step is set to a sufficiently small value $\tau_s = 10^{-5}$ s so that overlap due to a large increment in position can be avoided in one time step.

We simulate the motion of 200-400 molecules. The size of the simulation box is set so that an area fraction (equivalent to a concentration) can be achieved. It is well-known that concentration plays a role in phase separation. However, here, we do not aim to generate a phase diagram. Rather, our goal is specific to understanding the influence of interaction specificity on condensate features for a known concentration. That’s why, for the time being, we choose two values of area fractions a_f , 0.05 and 0.1, arbitrarily to test our model.

The diffusivity of the individual protein molecules is set to $D_p = 0.1 \mu\text{m}^2/\text{s}$. The value of diffusivity may appear very low. This low diffusivity has been reported earlier for RNA protein molecules inside the nucleus and cytoplasm [6, 7, 8]. However, it can be argued that the low diffusivity is because of the crowded and highly viscous environment inside the nucleus and cytoplasm. The actual diffusivity would differ if not crowded. It is apparent that, in phase separation, diffusion plays a key role for transporting the protein molecules. In our simulations, though there is no crowding, to keep the time scale for diffusion of the same order mimicking the environment of the nucleus and cytoplasm, we choose such a low value of diffusivity.

We use the sequential binding-unbinding model with the simulation framework mentioned above in a hybrid manner. When two protein molecules (whether part of clusters or individuals) are in close proximity, they bind with a sticking probability p_s and remain in a bound state for a lifetime that is randomly drawn from the PDFs shown in Fig. S1. The PDFs are generated for ranges of parameters shown in table S1. During the bound state, the molecules are part of clusters. The translational and rotational diffusivity of clusters are set to $D_c^t = D_p(r_p/r_c)$ and $D_c^r = D_c^t/(2r_c^2)$, respectively, where r_c is the radius of gyration of a cluster.

Table S1: Simulation parameters

mean time, τ_m	$N = 1$	$N = 5$	$N = 25$
15s	$\tilde{C} = 0.034$	$\tilde{C} = 0.3$	$\tilde{C} = 1$
130s	$\tilde{C} = 0.0038$	$\tilde{C} = 0.03$	$\tilde{C} = 0.047$

An accurate estimate of the sticking probability would be difficult, which would require a rigorous molecular dynamics simulation for a specific protein. However, here, we set $p_s = 0.1$ based on the following approximation. For a distance of d between two discs, the Van der Waals force experienced by each would be $|F_{vdw}| \sim (A/12)(r_p/d^2)$. Therefore, the potential energy barrier $\Delta U/(k_B T) \sim (F_{vdw} d)/(k_B T)$. Following Eyring’s theory [9, 10, 11], the sticking rate would be

$$k_s \sim (k_B T/h) \exp(-\Delta U/(k_B T)). \quad (\text{S7})$$

Here, A , k_B , T , and h are the Hamaker constant, Boltzmann constant, temperature, and Planck’s constant, respectively. The sticking probability for two discs at a distance d in one simulation time step is $p_s = 1 - \exp(-\tau_s k_s)$. For $A = 10^{-19}$ J (protein in water), $r_p = 5$ nm, $d = 0.5$ nm, $T = 303$ K, the sticking probability yields to $p_s = 0.1$.

Another variable in our simulations is the number of binding regions n_b per protein disc in 2D simulations. For example, if $n_b = 3$, it implies that a protein disc can allow a maximum of 3 other protein discs to be its neighbors in the bound state. We perform simulations for two values of n_b , 3 and 4.

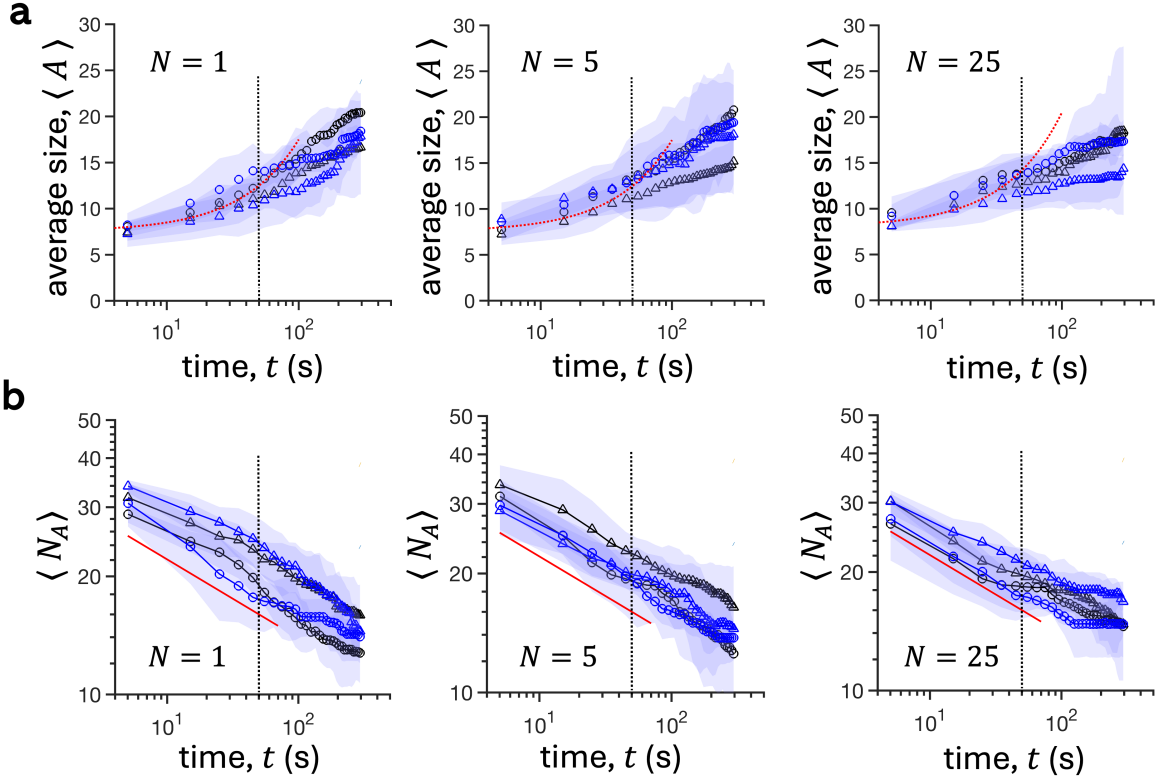


Figure S2: Variation of the mean size of clusters $\langle A \rangle$ with time t for different values of the total number of probable conformational changes N and the area fraction a_f . Here, the black and blue symbols are for the number of binding regions $n_b = 3$ and $n_b = 4$, respectively, and \circ and \triangle represent the mean lifetime of the lifetime distribution $\tau_m = 15$ s and $\tau_m = 130$ s, respectively. Panels in (a) and (b) correspond to $a_f = 0.05$, respectively. The red dotted curves ($y = mx + c$) fit the data points on the left of the black dotted vertical lines.

SI3 Counting number of neighbor exchanges

Counting the number of intra- and inter-cluster neighbor exchanges is difficult and a tricky job. We apply a simple approach as follows. When a molecule i is a part of a cluster, we track the ids j of the molecules bonded with i . For each i , we compare two sets of j collected at time t and after a window time $(t + \Delta t)$. These sets must be non-empty (an empty set represents that i is not part of a cluster). If these two non-empty sets are disjoint sets, which may imply that i is a part of either its old or a new cluster, we count one neighbor exchange event corresponding to i . The former follows the definition of a pure neighbor exchange event at the scale of an individual

molecule when it is a part of a cluster. In a similar manner, we perform this operation for rest of the molecules which are part of clusters, and count the total number of such events in that duration. We then obtain the cumulative total number of events at time (say, $(t + \Delta t)$), and this quantity is represented by N_{ex}^c .

References

- [1] Polyanin A. Handbook of linear partial differential equations for engineers and scientists; 2001.
- [2] Zaitsev V, Polyanin A. Handbook of exact solutions for ordinary differential equations; 2002.
- [3] Cichocki B, Hinsen K. Dynamic computer simulation of concentrated hard sphere suspensions: I. Simulation technique and mean square displacement data. *Physica A: Stat Mech Appl.* 1990;166:473-91.
- [4] Smith S, Cianci C, Grima R. Macromolecular crowding directs the motion of small molecules inside cells. *J Roy Soc Interface.* 2017;14:20170047.
- [5] Gu L, Wanunu M, Wang M, McReynolds L, Wang Y. Detection of miRNAs with a nanopore single-molecule counter. *Expert Rev Mol Diagnos.* 2012;12:573-84.
- [6] Tadakuma H, Ishihama Y, Shibuya T, Tani T, Funatsu T. Imaging of single mRNA molecules moving within a living cell nucleus. *Biochem Biophys Res Commun.* 2006;344:772-9.
- [7] Braga J, McNally J, Carmo-Fonseca M. A reaction-diffusion model to study RNA motion by quantitative fluorescence recovery after photobleaching. *Biophys J.* 2007;92:2694-703.
- [8] Chen J, Grunwald D, Sardo L, Galli A, et al. Cytoplasmic HIV-1 RNA is mainly

transported by diffusion in the presence or absence of Gag protein. Proceedings of the National Academy of Sciences. 2014;111:E5205-13.

- [9] Eyring H. The activated complex and the absolute rate of chemical reactions. Chem Rev. 1935;17:65-77.
- [10] Glasstone S, Laidler K, Eyring H. The theory of rate processes: the kinetics of chemical reactions, viscosity, diffusion and electrochemical phenomena. McGrawHill Book, New York. 1941.
- [11] Ball R, Weitz D, Witten T, Leyvraz F. Universal kinetics in reaction-limited aggregation. Phys Rev Lett. 1987;58:274.